Statistical Survey of Transition States and Conformational Substates of the Sperm Whale Myoglobin−CO Reaction System

Chong Zheng,*,‡ Vladimir Makarov,‡,§ and Peter G. Wolynes*,†

Contribution from the Departments of Chemistry, Northern Illinois University, DeKalb, Illinois 60115, and University of Illinois, Urbana, Illinois 61801

Received July 13, 1995. Revised Manuscript Received December 4, 1995[⊗]

Abstract: The distribution of activation energies for ligand rebinding in conformational substates of sperm whale myoglobin is investigated with a molecular dynamics−quenching method. The technique approximately locates transition states for curve crossing processes using an interpolating Hamiltonian as in Marcus's electron transfer theory. Linear free energy relations are examined. The transition from the dissociated state to the activated state involves a collective motion of the protein. The activation energy is correlated more to the extent of the collective motion of the protein than to the change of any single bond or bond angle. The predicted average structures of fast and slow rebinding substates which will soon be accessible to determination by cryogenic X-ray crystallography are compared. The CO geometry of the activated protein complex from the simulation agrees well with the structure of a low temperature photodissociated intermediate determined by Schlichting *et al.*

Introduction

The dynamic complexity of biomolecules in solution has been dramatically demonstrated by cryochemical studies of their reaction kinetics.[1−3] At physiological temperatures, many biological reactions can be effectively described by simple kinetic laws, but these conceal many steps in the biochemical transformations.[4,5] Low temperature kinetics unravels the individual steps by spreading them out in time scale[6,7] but simultaneously shows that there are a large number of distinct conformational substates which may have very different individual chemical reactivities.[8−11] The number of these conformational substates is sufficiently great that a statistical analysis of them is necessary for the interpretation of the experiments. The inhomogeneity of the configuration space of biomolecules has been confirmed by structural studies that show the existence of discrete conformations as well as large ranges of conformations as summarized in the Debye−Waller factors of X-ray diffraction.[12]

Computer simulations of biomolecules also confirm the existence of conformational substates.[13−20] Even over short periods of time, numerous distinct minima on the potential energy surface are sampled by molecular dynamics simulations. Although this is not a fair sample of all possible configurations, it does give one an idea of the lower bound of structural differences between conformational substates. The existence of conformational substates is a limiting feature in carrying out thermodynamic analyses of proteins via computer simulations. The inadequacy of sampling can mean that dynamically crucial conformations are missed in looking at protein reaction mechanisms. The sampling of conformational substates in many proteins has been shown to be adequate to explain the structural inhomogeneity as exhibited by the Debye−Waller factors. To our knowledge, previously no study of conformational substates by molecular dynamics simulations has sought directly to address their role in the inhomogeneity of the chemical kinetics, which is their most dramatic manifestation. As we shall see, this is a difficult undertaking involving the estimation of small enthalpy differences for large systems. An attempt in this direction, studying the role of conformational substates in the carbon monoxide dissociation reaction in sperm whale myoglobin, is the focus of this paper.

Method

A crucial issue which we seek to address is the possible structural origin of the kinetic inhomogeneity in protein reactions. It is important to realize that apparently small structural changes can have significant consequences for reaction barrier heights. Relatively small compressions of local structures can

* To whom correspondence should be addressed.
† Northern Illinois University.
‡ University of Illinois.
§ Present address: Baylor College of Medicine, Houston, TX 77030.
⊗ Abstract published in *Advance ACS Abstracts,* February 15, 1996.

(1) Austin, R. H.; Beeson, K. W.; Eisenstein, L.; Frauenfelder, H.; Gunsalus, I. C. *Biochemistry* **1975**, *14*, 5355.
(2) Frauenfelder, H.; Parak, F.; Young, R. D. *Annu. Rev. Biophys. Chem.* **1988**, *17*, 451.
(3) Frauenfelder, H.; Wolynes, P. G. *Science* **1987**, *229*, 337.
(4) Murray, L. P.; Hofrichter, J.; Henry, E. R.; Eaton, W. A. *Biophys. Chem.* **1988**, *29*, 63.
(5) Friedrich, J.; Gafert, J.; Zollfrank, J.; Vanderkooi, J.; Fidy, J. *Proc. Natl. Acad. Sci. U.S.A.* **1994**, *91*, 1029.
(6) Schlichting, I.; Berendzen, J.; Phillips, G. N., Jr.; Sweet, R. M. *Nature* **1994**, *371*, 808.
(7) Taubes, G. *Science* **1994**, *266*, 364.
(8) Frauenfelder, H.; Sligar, S. G.; Wolynes, P. G. *Science* **1991**, *254*, 1598.
(9) Steinbach, P. J.; Ansari, A.; Berendzen, J.; Braunstein, D.; Chu, K.; Cowen, B. R.; Ehrenstein, D.; Frauenfelder, H.; Johnson, J. B.; Lamb, D. C.; Luck, S.; Mourant, J. R.; Nienhaus, G. U.; Ormos, P.; Philipp, R.; Xie, A.; Young, R. D. *Biochemistry* **1991**, *30*, 3988.
(10) Nienhaus, G. U.; Mourant, J. R.; Frauenfelder, H. *Proc. Natl. Acad. Sci. U.S.A.* **1992**, *89*, 2902.
(11) Zhu, L.; Sage, J. T.; Champion, P. M. *Science* **1994**, *266*, 629.
(12) Ringe, D.; Petsko, G. A. *Prog. Biophys. Molec. Biol.* **1985**, *45*, 197.
(13) Levitt, M. *J. Mol. Biol.* **1983**, *168*, 621.
(14) Go, N.; Noguti, T. *Chem. Scr.* **1989**, *A 29*, 151.
(15) Elber, R.; Karplus, M. *J. Am. Chem. Soc.* **1990**, *112*, 9161.
(16) Straub, J. E.; Karplus, M. *Chem. Phys.* **1991**, *158*, 221.
(17) Straub, J. E.; Thirumalai, D. *Proteins: Structure, Function, and Genetics* **1993**, *15*, 360.
(18) Li, H.; Elber, R.; Straub, J. E. *J. Biol. Chem.* **1993**, *268*, 17908.
(19) Schaad, O.; Zhou, H.; Szabo, A.; Eaton, W. A.; Henry, E. R. *Proc. Natl. Acad. Sci. U.S.A.* **1993**, *90*, 9547.
(20) Straub, J. E.; Rashkin, A. B.; Thirumalai, D. *J. Am. Chem. Soc.* **1994**, *116*, 2049.

0002-7863/96/1518-2818$12.00/0

translate into chemically large energies. Similarly, changes of the electronic energy of reactant or product states caused by long-range forces and global perturbations of the structure can give significant changes in reaction rates. A major obstacle in studying chemical heterogeneity by computer simulation methods has been the difficulty of locating transition states for chemical reactions. The most natural approach to studying chemical heterogeneity would be to sample a variety of conformational substates of the reactant protein molecule as well as those of the final product state after the chemical change of covalent modification has occurred and then find the transition state between these two. Both the assignment of initial and final states and the finding of a bottleneck are difficult algorithmically.

Instead, the approach we take here is to locate approximately a series of transition state configurations and then to utilize ordinary quenching dynamics to discover which states these would go in reaction and from which states they originate. This strategy is most easy to apply for reactions that involve nonadiabatic curve crossing. Our approach was motivated by our earlier study of quantum effects on nonadiabatic electron transfer reactions.[21−23] Using path integral simulations techniques, we located conformation tunneling paths by simulating the protein with a Hamiltonian that interpolates between that of the product and reactant. A purely classical analog of this, in the case of electron transfer reactions, is to simulate the protein with a Hamiltonian corresponding to an intermediate state of charge, just as in the Marcus theory of electron transfer.[24] After a long simulation is carried out, one can quench the system to a minimum on the partially charged potential energy surface. In the classical Marcus picture, this corresponds to finding the minimum on the excited state potential energy surface. For a locally harmonic Hamiltonian, this would be very close to the transition state for the reaction, and, indeed, one can easily find a nearby crossing to any state prepared in this way. After a sequence of such transition states is obtained, a further quenching of each transition state can be carried out on the reactant and product energy surfaces leading to an assignment of both reactant (deoxy myoglobin), product (myoglobin−CO), and transition state (myoglobin···CO). The procedure is shown schematically in Figure 1.

It is relevant to point out that the Marcus intermediate charging strategy, while most appropriate for quasi-harmonic models, is a natural first approximation for any nonadiabatic process. The notion is implicit in Jortner and Ulstrup's treatment[25] of ligand recombination in heme proteins. While Frauenfelder and one of us have argued elsewhere[3] that ligand recombination is actually adiabatic, estimation of the splitting at the curve crossing would suggest that the energy splitting is not so large as to greatly change the location of transition states. In any case a detailed quantum chemical treatment including the location of the triplet states is desirable to settle this. Such a treatment is beyond the scope of this study.

This quenching simulation was carried out in this study for the dissociation reaction of carbonmonoxy myoglobin. The Hamiltonian we used in the simulations was of the GROMOS type,[26] with the heme coordination parameters modified to fit the experimental X-ray structures of the bounded and dissociated

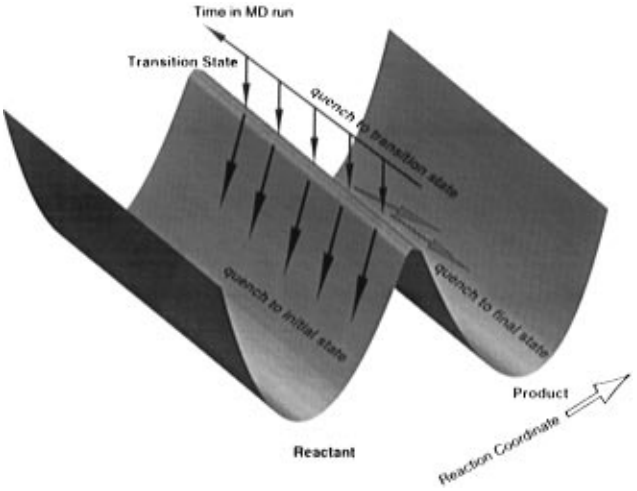

Figure 1. Schematic representation of the quenching procedure. The system is initially quenched to the transition state described by an interpolated Hamiltonian and then to the reactant and product surfaces.

states (see the Appendix). The atomic charges were scaled according to their distances from the center of the protein to mimic the solvent screening effect.[27] Nonbonded interactions were truncated by multiplying the potential functions by the atom-based shifting function

$$S(r) = \begin{cases} 1 - (r^2/r_c^2)^2, & 0 < r \le r_c \\ 0, & r_c < r \end{cases}$$

The cutoff radius in our simulations was 12 Å. This atom-based shifting function has been shown to be superior to the traditional smoothing function.[28] The crystal structure of sperm whale myoglobin determined by Kuriyan, Wilz, Karplus, and Petsko was taken from the Protein Data Bank.[29] After polar hydrogen atoms were added, the protein structure was prepared through conjugated gradient energy minimization (1000 steps) and standard thermalization steps (50 ps with 1 fs step size). We used a Morse potential of the Straub−Karplus type to describe the C−O interaction.[16] The bound state was modeled by a Morse potential and the dissociated state by a repulsive exponential function first used by Agmon and Hopfield[30]

$$V(r) = \begin{cases} V_s = D_e[\exp(-2\beta r) - 2\exp(-\beta r)], & \textit{bound state} \\ V_q = D_e[\exp(-\beta r) - \Delta], & \textit{dissociated state} \end{cases} \quad (1)$$

where r is the Fe−C distance, $\beta = 1.5$ au^{-1}, and D_e and Δ are fitted to experimental data: $D_e = 138$ kJ/mol, $\Delta = 26$ kJ/mol. V_s is the potential function for the bound state in which the spin state of Fe is singlet. V_q is for the dissociated state with a quintet spin state. This form of potential has been successfully applied by Li, Elber, and Straub in a molecular dynamics study of the dissociation reaction of NO in mutant myoglobin.[18] Free energy of dissociation was calculated using the free-energy perturbation method,[31] with the charging parameter $\lambda = 0$ corresponding to carbonmonoxy myoglobin (myoglobin−CO) and $\lambda = 1$ to deoxy myoglobin. We fitted the Morse potential parameters to the experimental activation energy of 11 kJ/mol.[3]

(21) Zheng, C.; Wong, C. F.; McCammon, J. A.; Wolynes, P. G. *Nature* **1988**, *334*, 726.
(22) Zheng, C.; McCammon, J. A.; Wolynes, P. G. *Proc. Natl. Acad. Sci. U.S.A.* **1989**, *86*, 6441.
(23) Zheng, C.; McCammon, J. A.; Wolynes, P. G. *Chem. Phys.* **1991**, *158*, 261.
(24) Marcus, R. A. *Angew. Chem., Int. Ed. Engl.* **1993**, *32*, 1111.
(25) Jortner, J.; Ulstrup, J. *J. Am. Chem. Soc.* **1979**, *101*, 3744.
(26) van Gunsteren, W. F.; Berendsen, H. J. C.; Hermans, J.; Hol, W. G. J.; Postma, J. P. M. *Proc. Natl. Acad. Sci. U.S.A.* **1983**, *80*, 4315.
(27) Northrup, S. H.; Pear, M. R.; Morgan, J. D.; McCammon, J. A.; Karplus, M. *J. Mol. Biol.* **1981**, *153*, 1087.
(28) Steinbach, P. J.; Brooks, B. R. *J. Comput. Chem.* **1994**, *15*, 667.
(29) Kuriyan, J.; Wilz, S.; Karplus, M.; Petsko, G. A. *J. Mol. Biol.* **1986**, *192*, 133.
(30) Agmon, N.; Hopfield, J. J. *J. Chem. Phys.* **1983**, *79*, 2042.
(31) Straatsma, T. P.; McCammon, J. A. *Annu. Rev. Phys. Chem.* **1992**, 407.

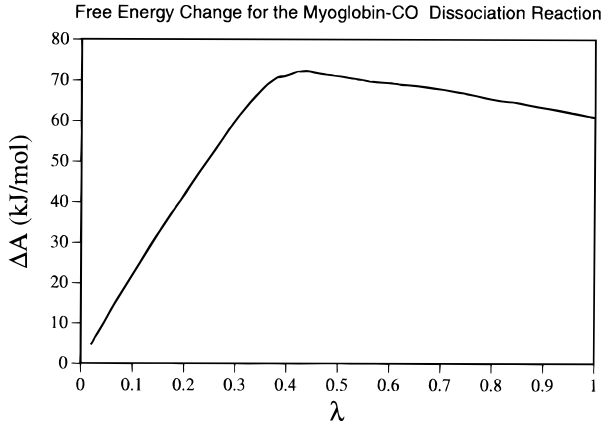

Figure 2. Free energy as a function of the charging parameter λ. $\lambda = 0$ corresponds to carbon monoxy myoglobin and $\lambda = 1$ deoxy myoglobin. The transition state is at $\lambda = 0.44$.

Five subsequent free energy perturbation runs were carried out, and the average free energy profile from these runs was obtained (Figure 2). The transition state was determined from this profile to be at $\lambda = 0.44 \pm 0.02$ with activation free energy 11 ± 3 kJ/mol. The system was then subjected to a 50 ps (1 fs/step) equilibration run at the transition state at 300 K before data collection. A 50 ps data collection run was carried out afterwards. The transition state conformation was recorded at every 100 fs followed by a quenching to a local minimum on the transition state potential surface. This state was again quenched to local minima at the reactant and product potential surfaces. The quench procedure we used was a steepest descent energy minimization run terminated when energies of successive steps differed in less than 0.1 kJ/mol. Similar sampling runs were carried at other temperatures (10 and 600 K).

Using this approach, we obtained, thereby, a sampling of transition states and the initial conformational substates from which they arise. We are thus able to get some idea of the distribution of barrier heights. In addition, we can correlate individual barriers with changes in reactant and product energies as well as look at the structural causes of kinetic heterogeneity. The CO dissociation reaction is easy to study by this method because of the relative ease of finding effective potential energy surfaces. The same technique can be applied to other reactions such as the carbon monoxide recombination to cytochrome *c*, once an appropriate model of the two surfaces is available from quantum chemical calculations and experimental measurement.[32]

A technical issue which faces us in evaluating the distribution of activation energies is noise generated by the numerical minimization method. In a large enough anharmonic system distant regions from the active site may be near to saddle points for configurational motion, and errors in minimization determine to which side of the local saddle the system falls on quenching. Although this will not change the structure very much at the active site, it will introduce an absolute error in the energy which is considerable when taking differences. Apparently this occurs when we use the total energies in determining the activation energy distribution. In particular the noise from the electrostatic interaction is significant and of order 11 kJ/mol. We used an 8 Å cutoff sphere around the CO in evaluating the energy differences. This interaction region shown in Figure 12 does not include those surface residues far from the active site but does contain 21 residues close to the active site including the proximal and distal histidines. As the interaction sphere is extended beyond this point there is increasing sensitivity to minimization noise and considerable broadening of the activation energy distribution.

(32) Bren, K.; Gray, H. B. *J. Am. Chem. Soc.* **1993**, *115*, 10382.

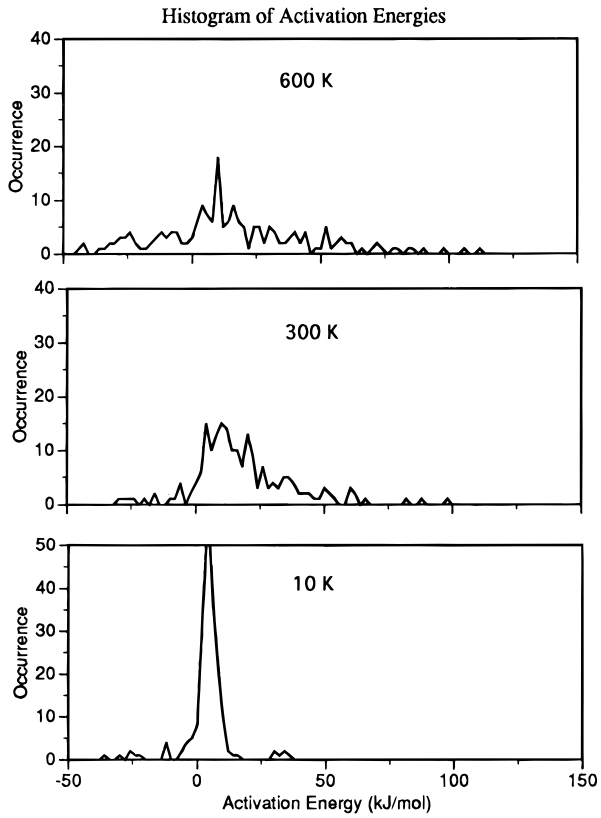

Figure 3. Histogram of activation energies at various temperatures.

Results and Discussion

Distribution of Barrier Heights. The histogram of the activation energy barrier for the CO dissociation reaction is shown in Figure 3. The survey is conducted for 200 substates each on the reactant, transition and product surfaces, and the activation energies calculated as the difference of energies between the transition and reactant states. The increase of the distribution width with temperature reflects a larger fluctuation of the protein structure at higher temperature. It also contains more errors because of the larger fluctuation. The distribution at low temperature (10 K) has a width similar to the experimentally determined value ($\sim$20 kJ/mol).[9] The peak position is around 10 kJ/mol at 300 K, compared to the overall activation barrier of 11 kJ/mol.[3] The negative tail and the near zero values of the distribution are largely due to noise. They disappear if the cutoff radius for the computation of activation energies is less than 5 Å. The distribution width at 300 K is larger than the experimental value, also due to the noise produced by the cutoff and other approximations.

Linear Free Energy Relationship. The activation energy is plotted against the difference of the energies of the initial (dissociated) and final (bound) states in Figure 4. Each dot in the figure represents a triplet of initial, transition, and final states obtained by the quenching procedure mentioned above. As temperature increases and more substates are accessible, the dots are more delocalized in the graph. The slope of the least-squared fitted line changes from 0.47 at 10 K to 0.64 and 0.56 at 300 and 600 K, respectively. The slope is close to the classical Marcus value of 0.5, indicating that the transition is in the normal region. In Marcus theory, the activation free energy ΔG^* depends quadratically on the difference of free energies between the product and reactant, ΔG^0

$$\Delta G^* = \frac{\lambda}{4}\left(1 + \frac{\Delta G^0}{\lambda}\right)^2$$

In the normal region, ΔG^0 is usually much smaller than the

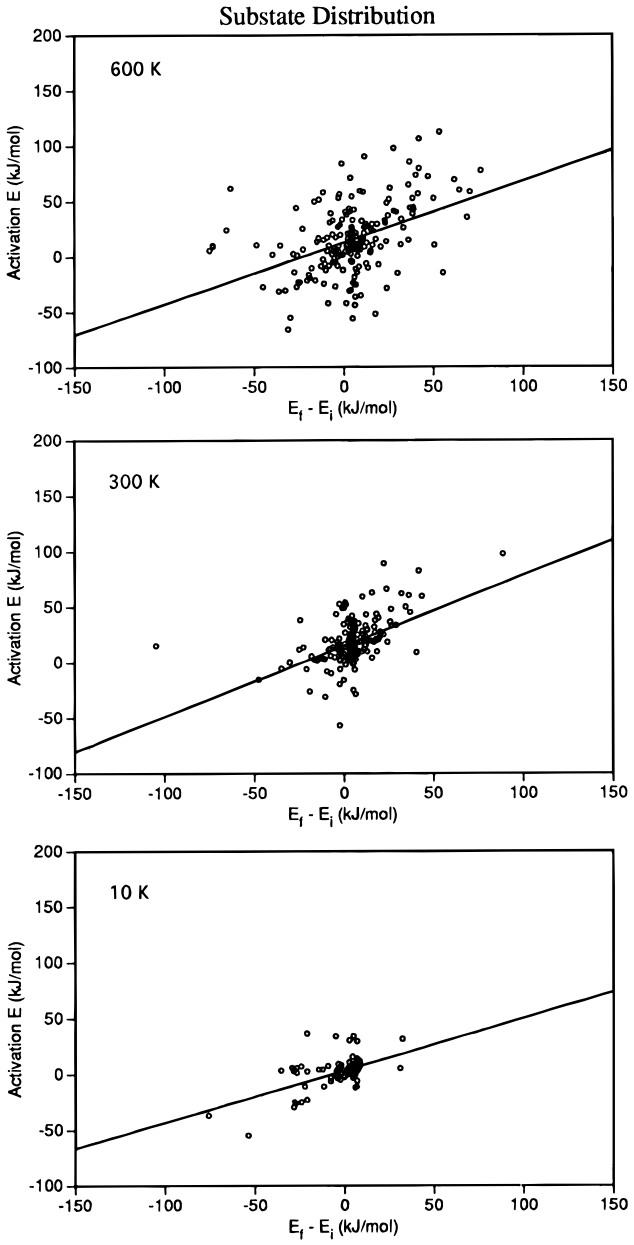

Figure 4. Activation energy vs the energy difference between the initial (deoxy myoglobin) and final (carbonmonoxy myoglobin) states at various temperatures. The straight lines are least-square fits.

reorganization energy λ. A first order approximation of the equation thus yields a slope of 0.5.

Transition to Transition State and to Connecting Substate. The microscopic motions of the protein atoms during the transitions are summarized in Figures 5 and 6. Figure 5 is the histogram of the participation number of the transitions between the adjacent, connecting substates on the reactant (dissociated CO) surface. The participation number P is defined as

$$P = N\frac{|\langle \Delta r^2 \rangle|^2}{\langle \Delta r^4 \rangle}$$

where N is total number of atoms in the protein and Δr the individual atomic displacement during a transition, the average <...> is taken over all atoms in the protein. If the displacement is localized in a few atoms, P will be the order of one.[33,34] On the other hand, if the displacement is widely spread in the protein, P will be of the order of the total number of atoms in the protein. The participation number was calculated after the overall translational and rotational motions of the protein were removed using a least-square fitting procedure.

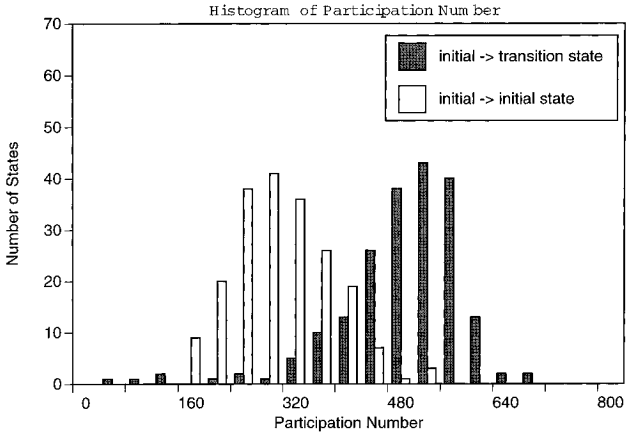

Figure 5. Histogram of the participation number of the 200 quenched substates.

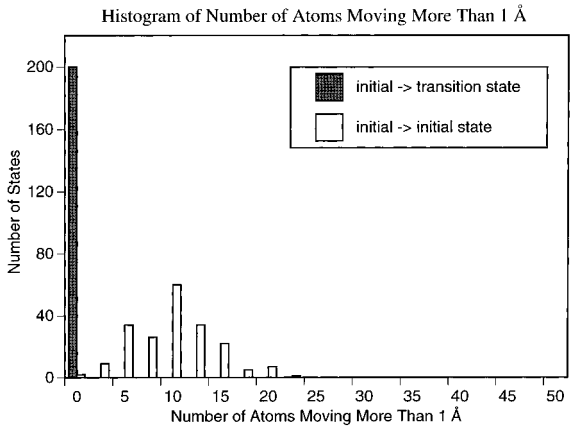

Figure 6. Histogram of the number of atoms moving more than 1 Å for the 200 quenched substates.

The histogram of the participation number in Figure 5 was calculated using the 200 triplets obtained by the quenching procedure mentioned above. The participation number for a transition from one substate to another was calculated only for adjacent substates separated by the 100 fs interval in the simulation. During this short time, we assume that the substates are connected in the sense that they can make a transition to each other without going through a third one. Figure 5 shows that the atomic motion of the transition from an initial substate (dissociated CO) to the transition state is more widely spread in the protein, whereas a transition to a connecting substate on the reactant (dissociated CO) surface is more localized, possibly involves a motion of a side chain or a rotation of a functional group. The RMS displacement of the atoms within the 8 Å pocket of CO is about 0.4 Å, while that of the atoms of the whole protein is about 0.3 Å. In addition, Figure 6 shows that although the structural difference between substates on the initial potential surface is more localized, there are more atoms moving larger distance (greater than 1 Å). A transition to an activated state, however, is more of a collective motion involving more atoms with each moving at a small distance. The RMS displacement of the atoms in the 8 Å pocket of CO as well as in the whole protein is about 0.1 Å. For comparison, the RMS atomic displacement between the reduced and oxidized tuna cytochrome *c* structures is about 0.5 Å,[35] and the atomic displacement in an $\alpha\beta$ subunit of the R and T states of

(33) Stillinger, F. H.; Weber, T. A. *Phys. Rev. A* **1983**, *28*, 2408.
(34) Ohmine, I.; Tanaka, H.; Wolynes, P. G. *J. Chem. Phys.* **1988**, *89*, 5852.
(35) Takano, T.; Dickerson, R. E. *J. Mol. Biol.* **1981**, *153*, 95.

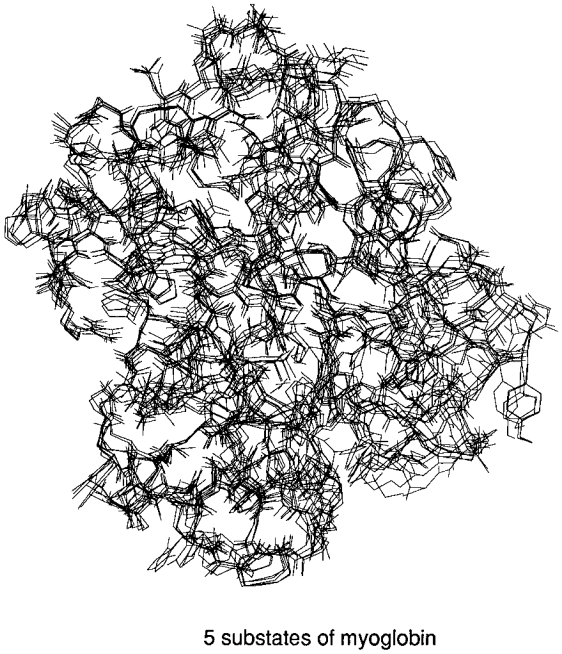

Figure 7. Five quenched sperm whale myoglobin substates on the product (bound CO) potential surface.

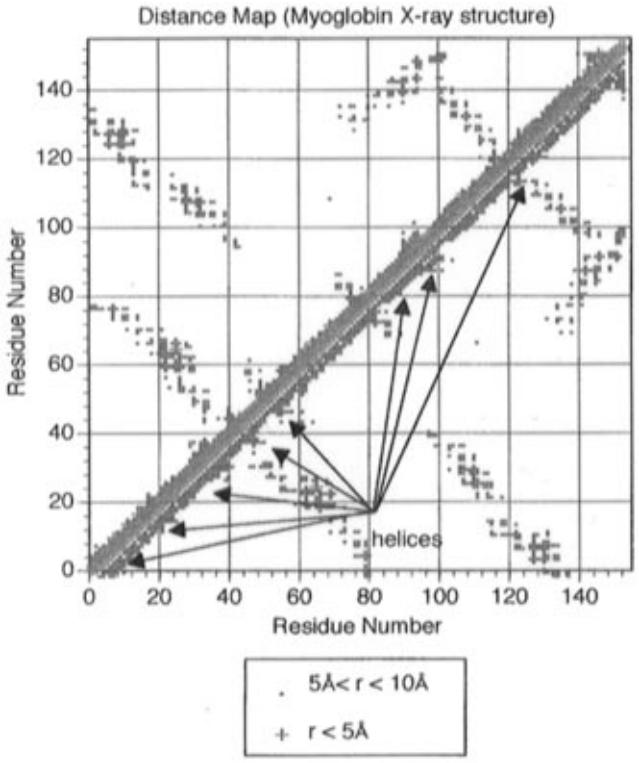

Figure 8. Distant map of the C_α atoms of the 1.5 Å sperm whale myoglobin X-ray structure.

hemoglobin is about 0.8 Å.[36] Figure 7 shows five substates on the final potential (bound CO) surface (translational and rotation motions of the protein were removed). The largest difference is in the side chains.

The structural difference between the substates on the initial surface can be quantified using the distance map. The distance map of the 1.5 Å X-ray crystal structure of sperm whale is shown in Figure 8. It is a plot of the distances between the C_α atoms of all the residues. Various islands in this plot are associated to the secondary structures in the protein.[37] For example, the distance between *i*th and (*i*+4)th C_α atoms in an a-helix can be close to 5 Å. Similarly, the distance between C_α atoms in a turn can also be short. This protein has eight helices, starting at Ser3, Asp20, His36, Thr51, Ser58, Leu86, Pro100, and Gly124. The helices consist of about 75% of the main chain, thus the protein is rather rigid. These helix regions are close to the diagonal in the map (off by about 3−4 residues). The same type of description can be used for $C_\alpha-C_\alpha$ distance fluctuations between substates. Figure 9 is the $C_\alpha-C_\alpha$ distance fluctuation map of the 200 myoglobin substates on the product surface (bound CO). Only fluctuations larger than 1 Å are plotted. Two features in the plot stand out. First, there are more C_γ fluctuations than C_α. It is expected because side chains are more flexible than the backbone of the protein. Secondly, the larger fluctuations are not in the helices and turns, as they are more rigid than the loops. Similar patterns are also observed for substates on the transition and the reactant potential surfaces.

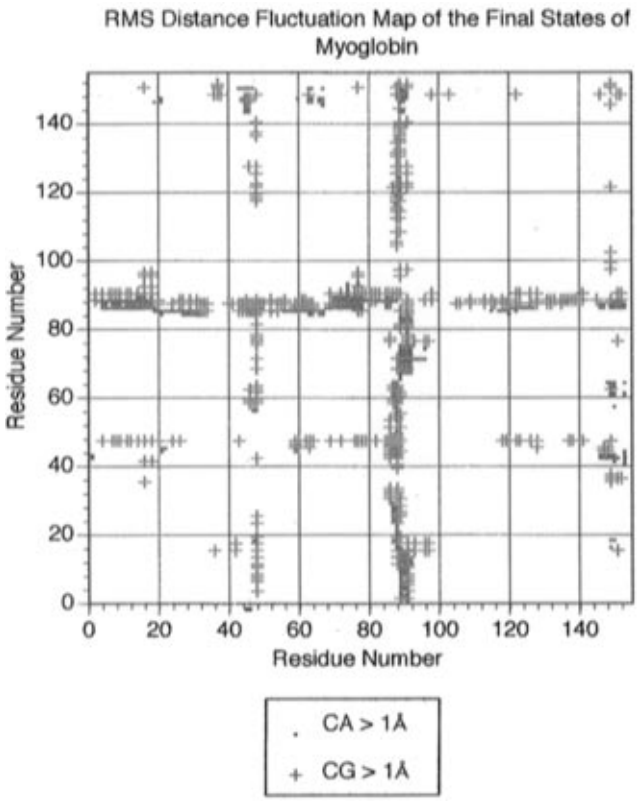

Figure 9. Map of the RMS distant fluctuations in the substates of sperm whale myoglobin in the product (bound CO) surface. Only C_α and C_γ fluctuations with RMS greater than 1 Å are shown.

Correlation between Structural Change and Activation Energy. Low temperature X-ray crystallography has become one of the most powerful tools to study protein conformation change during enzyme catalysis. The structure of the activated complex, for example, can be obtained by X-ray crystallographic method at low temperature when the lifetime of the complex is sufficiently long.[6] It is therefore important to ask which conformation is associated with high activation energy and which with low activation energy. The correlation between the activation energy and the change of the heme geometry is plotted in Figure 10. Five parameters were used to investigate the correlation. The first is the change of Fe−C distance ΔR_{Fe-C} when the dissociated complex is activated at the transition state. The correlation is plotted in the top panel of Figure 10. Each dot represents a pair of conformations (dissociated and transition state) from which the activation energy and ΔR_{Fe-C} are

(36) Baldwin, J.; Chothia, C. *J. Mol. Biol.* **1979**, *129*, 175.

(37) Richards, F. M.; Kundrot, C. E. *Proteins: Struct. Funct. Genet.* **1988**, *3*, 71.

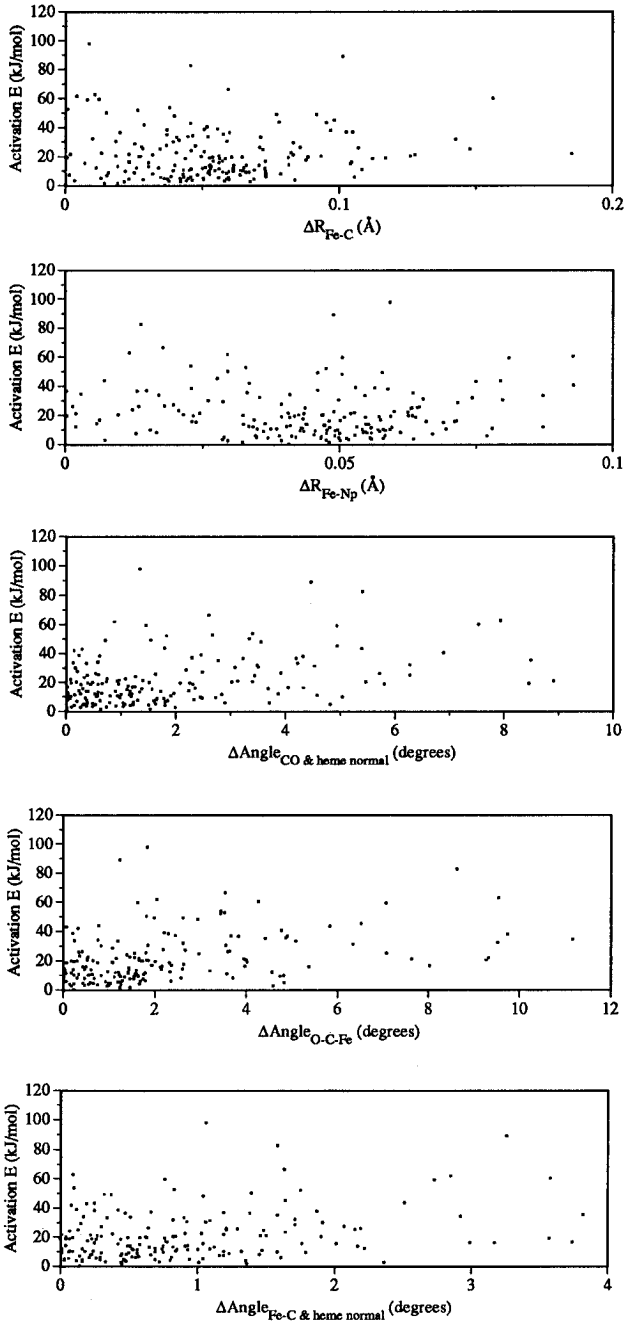

Figure 10. Scatter plot showing the correlation between the activation energy and the change of heme geometry in the activation process. The local bond length and bond angle charges are: $\Delta R_{\mathrm{Fe-C}}$: the change of the Fe−C bond; $\Delta R_{\mathrm{Fe-Np}}$: the change of the distance from Fe to the plane defined by the pyrrole nitrogen atoms; $\Delta\mathrm{Angle}_{\mathrm{O-C-Fe}}$: the O−C−Fe angle change; and $\Delta\mathrm{Angle}_{\mathrm{Fe-C\ and\ heme\ normal}}$: the change of the angle between the Fe−C bond and the heme normal.

calculated by the simulation. From the graph it can be seen that there is only a weak correlation, small $\Delta R_{\mathrm{Fe-C}}$ can have both large and small activation energies. The same is true for other parameters: the change of the distance from Fe to the plane defined by the pyrrole nitrogen atoms, $\Delta R_{\mathrm{Fe-Np}}$; the O−C−Fe angle change, $\Delta\mathrm{Angle}_{\mathrm{O-C-Fe}}$; and the change of the angle between Fe−C bond and heme normal, $\Delta\mathrm{Angle}_{\mathrm{Fe-C\ and\ heme\ normal}}$. However, the correlation between the number of atoms moving a large distance and the activation energy in an activation process is much more significant, as is shown Figure 11. Since the correlation is more probabilistic than deterministic, an intrinsic feature of substates of proteins and glasses, we show both the individual and an average correlation. Thus in Figure 11, the dots are the plot of the

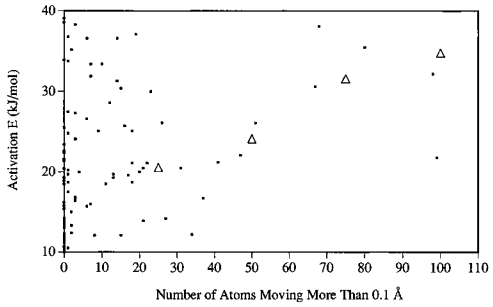

Figure 11. Activation energy as a function of the number of atoms moving more than 0.1 Å (dots). The triangles represent the activation energies averaged for substates in a 25 kJ/mol interval.

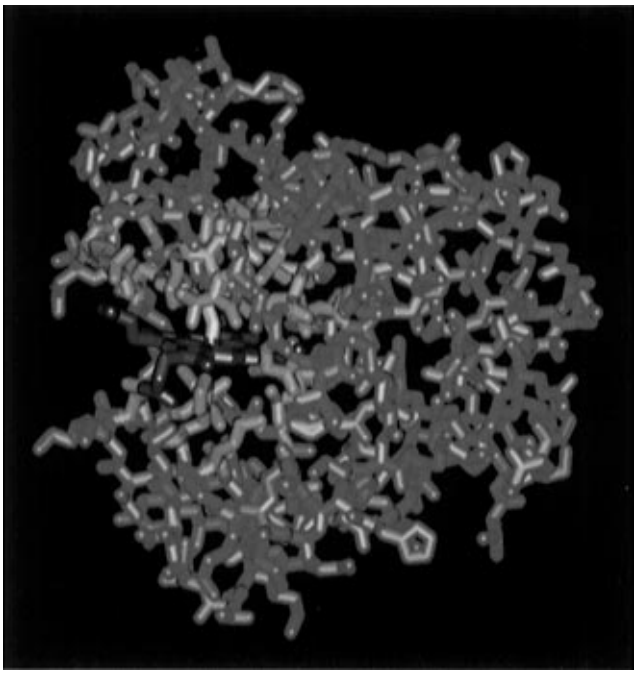

Figure 12. The X-ray crystal structure of the sperm whale carbonmonoxy myoglobin. The heme group is in red color, and the residues within the 8 Å sphere of the CO are in blue.

activation energy as a function of the number of atoms moving more than 0.1 Å for each individual substate, whereas the triangles represents the activation energies averaged for all substate pairs with activation energy within a 25 kJ/mol interval. It is clear in this figure that the activation energy is likely to be larger when more atoms are involved in large amplitude motions. It is the atoms around the heme group that are responsible for the activation process, and the number of these atoms is around the order of a few tens. From Figures 10 and 11, we can say that the activation process is a collective motion involving many atoms.

Heme Geometry of the Activated Substates. Recent advances in X-ray techniques at liquid-helium temperature have made it possible to obtain protein structures during biological reactions. Schlichting *et al*. have determined the structure of an intermediate, transition state of the myoglobin−CO dissociation reaction.[6] One of the main differences between the intermediate and the final carbon monoxy structures is the angle between the CO bond and the heme normal. In the intermediate structure, the angle is 91 degrees, i.e., CO lies rather parallel to the heme plane. The IR result of 80 ± 10 degrees also supports this fact. In the carbon monoxy structure the angle is 32 degrees, rather perpendicular to the heme plane. To examine the validity of our model, we analyzed the 200 activated substates. The CO−heme geometry obtained is compared with the low-temperature X-ray structure in Table 1. It is clear that

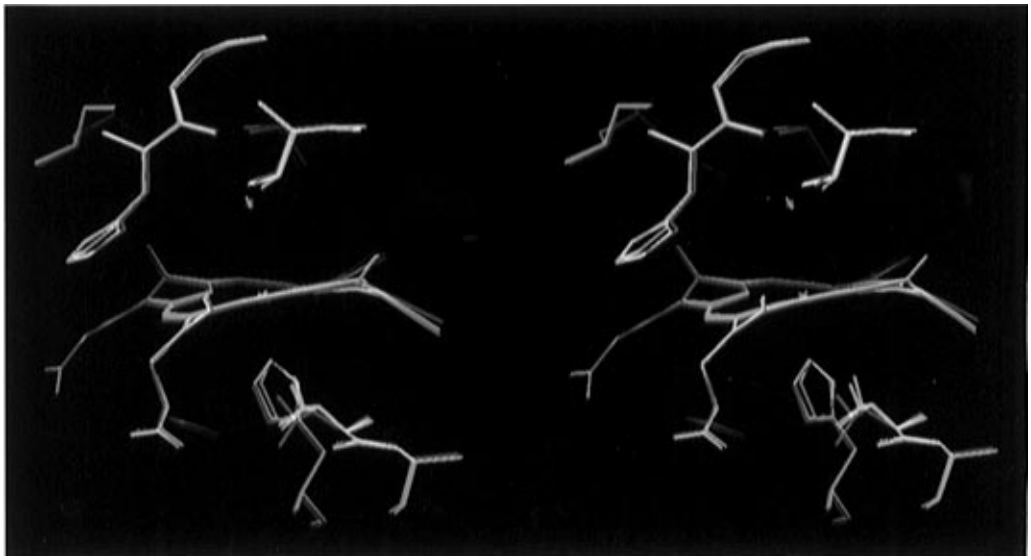

Figure 13. Average structures of substates with activation energies between 0 and 12 kJ/mol (blue), between 12 and 24 kJ/mol (green), and between 24 and 36 kJ/mol (red).

Table 1. Heme Geometry of the Activated Substates

	X-ray	simulation
angle between CO bond and heme normal (deg)	91	73 ± 36
O−C−Fe angle (deg)	111	104 ± 39
angle between Fe−C bond and heme normal	39	14 ± 9
Fe−C distance (Å)[a]	4.14	3.0 ± 0.6
Fe−O distance (Å)	3.60	3.3 ± 0.6
Fe−Np plane distance (Å)	0.19	0.09 ± 0.07
⟨Fe−Np⟩ (Å)	1.98	1.99 ± 0.04
Fe−$N^{\epsilon 2}$ (proximal his) (Å)	2.25	2.16 ± 0.04
angle between Fe−$N^{\epsilon 2}$ (proximal his) and heme normal	3.3	9 ± 5

[a] The X-ray structure assumed that O is closer to Fe than C, opposite to our simulation set-up. The X-ray data do not exclude the possibility that C is closer to Fe.

Table 2. Modified GROMOS Force Parameters

	myoglobin−CO	deoxy myoglobin
NR5−Fe (Å)	2.19	2.10
NP−Fe (Å)	1.98	2.02
NR5−Fe−NP (deg)	90	100
NP−Fe−NP (deg)	90	88

our model catches the essential feature of the activation geometry, i.e., CO is more parallel than perpendicular to the heme plane. The O−C−Fe angle obtained by our simulation is also close to the experimental value. The Fe−C and Fe−O distances, however, are slightly shorter than the experimental data, possibly due to the limited simulation time and unrelaxed protein structure in the activated state. Note that the experimental structure assumes that O is closer to Fe than C, opposite to our simulation set-up. However, the experimental data do not exclude the possibility that C is closer to Fe. Our simulation also indicates that CO can rotate rather freely above the heme plane.

Activation Energy and Its Correlation to the Heme Geometry of the Intermediate Species. One of the most intriguing issues that the time-resolved X-ray crystallography concerns is the connection between the structure and association rate of the CO to the protein. Since the association rate is determined by the activation energy, we should examine the structural difference between the intermediate species possessing different activation energies. The structures averaged over three activation ranges are shown in Figure 13. Only the heme pocket is shown as the activation energies were calculated using the residues in this vicinity. The blue is the structure averaged for all substates with activation energies between 0 and 12 kJ/mol, the green is the average structure of substates with activation energies between 12 and 24 kJ/mol, and the red with activation energies between 24 and 36 kJ/mol. Within the framework of our quenching model, we can see that the proximal histidine tilts more to the side of the propionate chains of the heme for the structures with higher activation energies. The distal histidine also bends more toward the heme plane for the structure with higher activation energy. This seems in disagreement with the experimental observation that the angle between the Fe−N^{e2} (proximal histidine) bond and the heme normal decreases upon activation, but in fact there is no contradiction, since the substates with smaller tilt will be favored as they have lower activation energy. Furthermore, the Fe−C−O angle decreases as the activation energy increases. Other residues that shift significantly with activation energy are Leu 86, Pro 88, and Leu 89. The most significant shift is of the order of 0.8 Å, larger than the RMS deviation of 0.3−0.4 Å of structures within the same activation energy interval. However, our simulation did not reproduce the displacements of Phe 43 and Leu 29 that were observed experimentally. It would be interesting to see if our prediction based on a very approximate model agrees with future experimental measurements.

Appendix

The modified GROMOS force parameters are listed in Table 2.

Acknowledgment. This work was also supported in part by NSF Grant CHE-92-23244 to P.W.G. and through a Presidential Young Investigator Grant (CHE-91-57717) awarded to C.Z. Part of the computations were carried out at the National Center for Supercomputing Applications at University of Illinois at Urbana-Champaign.

JA9523092